NUCLEAR SCIENCE AND ENGINEERING: **178**, 459–478 (2014)

The Evaluation of the Effective Kinetic Parameters and Reactivity of the IPEN/MB-01 Reactor for the International Reactor Physics Experiment Evaluation Project

Adimir dos Santos* and Ricardo Diniz

Instituto de Pesquisas Energéticas e Nucleares – IPEN/CNEN-SP, Av. Prof. Lineu Prestes 2242, Cidade Universitária, São Paulo, Brazil, 05508-000

Received January 10, 2014
Accepted June 17, 2014
http://dx.doi.org/10.13182/NSE14-10

Abstract—*The evaluation of the experiments of the effective delayed neutron parameters and reactivity performed in the IPEN/MB-01 research reactor facility has been successfully accomplished. The evaluated data are of very good quality and fulfill the requirements of a benchmark. The recently released MCNP6 together with the ENDF/B-VII.1, JENDL-4.0, JEFF-3.1.1, ENDF/B-VII.0, and JENDL-3.3 nuclear data libraries has been employed to calculate the effective delayed neutron parameters adopting the benchmark model of the IPEN/MB-01 reactor available in the International Handbook of Reactor Physics Benchmark Experiments. The analysis reveals that all these nuclear data libraries produced satisfactory results for* β_{eff}, β_{eff}/Λ, *and* Λ. *The same cannot be said for determining the reactivity using the Inhour equation. It was shown that there is a clear tendency to increase the deviation with the absolute value of the reactivity for negative periods. Only JENDL-3.3 and JEFF-3.1.1 produced results that are inside the* 3σ *range of the benchmark value uncertainty. Specifically for the case of ENDF/B-VII.1, a good part of this discrepancy is due to the decay constant of the first group of delayed neutrons, which is overestimated according to the experimental value measured in the IPEN/MB-01 reactor.*

I. INTRODUCTION

Since the first stages in the development of fission chain reactors, the importance of reactor physics experiments has been recognized. For many years, reactor physics experiments[1–17] have been carried out worldwide, and very valuable experimental data have been published to serve as benchmarks. They constitute an essential tool for reactor physicists for validating calculation methodologies and related nuclear data libraries. The great majority of reactor physics experiments belong to the category of critical mass and the related spectral index. With the availability of modern acquisition boards and more accurate equipment, new experimental techniques[11–17] have been developed for determining very important reactor physics parameters such as the effective delayed neutron fraction β_{eff} and the relative abundances of delayed neutrons β_i/β_{eff} and subcritical measurements. Up to a few years ago, the most famous reactor physics experiments were the ones chosen by the Cross Section Evaluation Working Group[1] (CSEWG). Numerous researchers[18–22] have assessed the CSEWG benchmarks and several other experiments in widely varying situations.

Since the advent of the International Criticality Safety Benchmark Evaluation Project[23] (ICSBEP) in 1992 and, more recently, the International Reactor Physics Experiment Evaluation Project[24] (IRPhEP), the evaluation of criticality safety and reactor physics benchmark experiments has experienced tremendous growth. The ICSBEP and IRPhEP committees have been continuously providing a standard basis for criticality safety and reactor physics benchmark evaluations. At the same time, the scope, the diversity, and

*E-mail: asantos@ipen.br

the quantity of benchmarks available to the reactor physics community have significantly increased from year to year. Moreover, the ICSBEP and IRPhEP committees are stimulating the development of new experimental techniques as well as new approaches to treat the uncertainties arising from the experiments and from the geometric and material data of the facilities. The impact of the ICSBEP and IRPhEP evaluations on several branches of reactor physics has been enormous. For example, the work of the ICSBEP and IRPhEP committees has been of great benefit in the development of ENDF/B libraries. Numerous recent works based on the ICSBEP and IRPhEP evaluations[25–28] have assessed the quality of the nuclear data contained in the versions and releases of the ENDF/B libraries. Particularly, while providing a standard basis for the cross sections needed for the theoretical analysis of reactor physics experiments in general, the development of the ENDF/B libraries also necessitates the development of very sophisticated mathematical and computational methods on one hand and specific and accurate evaluation of experiments on the other hand. At the same time that the scope, the quality, and the quantity of nuclear data (for example, the number of resolved resonances) have significantly increased from nuclear data library version to version, advances in the computer technologies, as well as in the mathematical and computational techniques both in the preprocessing codes and in the solution of the neutron transport equation, have allowed one to perform very detailed calculations using sophisticated codes. Nowadays, mathematical and computational techniques have matured to such a state of development that the main uncertainty in the nuclear reactor calculations is believed to be in the basic nuclear data. From this viewpoint, it is very important that experiments designed to serve as benchmarks to validate calculation methodologies and related nuclear data libraries introduce uncertainties that are smaller than those in the calculated reactor responses due to the basic nuclear data. It is in the former that the ICSBEP and IRPhEP committees have been successful in the last several years through the evaluation, dissemination, and establishment of several high-quality benchmark problems in widely varying applications.

Among the several integral reactor physics parameters commonly measured in critical facilities, effective delayed neutron parameters like β_{eff} play an important role because they have an important bearing on the dynamic behavior of a nuclear reactor. Particularly, knowledge of β_{eff} is essential for normalization of the reactivity and for the time characteristics of transients. Up to a few years ago calculation/experiment discrepancies in measurements of the effective delayed neutron fraction β_{eff} were undesirable in design and operation of reactor control systems.[29] More precisely, a target accuracy of $\pm 3\%$ (1σ) has been requested for the experimental β_{eff} (Ref. 30). For β_{eff} calculations, the target accuracy that has been proposed is also $\pm 3\%$ (1σ) (Refs. 31 and 32). Until recently, this accuracy in calculations was more clearly met for fast reactors than for thermal reactors because there were fewer measurements of β_{eff} available for validating the calculations for thermal systems.[33,34] However, with more new measurements performed in the IPEN/MB-01 research reactor facility[11–14] (IPEN/MB-01 facility) and with the availability of the MISTRAL experiments[15] performed in Cadarache, this goal has also been achieved for thermal reactors.

In contrast to other techniques like the Slope Method,[9] Nelson-Number Method,[9] and ^{252}Cf-Source Method,[35] the main advantage of these new experimental methodologies developed at the IPEN/MB-01 facility is to obtain the effective delayed neutron parameters in a purely experimental way, eliminating all parameters that are difficult to measure or calculate. Consequently, the uncertainties associated with these parameters are eliminated, and the accuracy in the effective delayed neutron parameters is improved. These techniques are based on macroscopic and microscopic noise. The macroscopic noise experiments exploit the very low-frequency range (< 1.0 Hz) and show that that it is possible to resolve the low-frequency region and extract very useful information from there. The microscopic noise experiments are based on the two-region model[36] (reflected-core kinetic model) and rely on the measurements of Rossi-α (Ref. 37) and Feynman-α (Ref. 38) distributions at several subcritical levels. Both techniques are claimed to be well defined and produced experimental data of very high quality. Finally, as a product of this set of experiments, benchmark values for β_{eff} and the prompt neutron generation time Λ, their ratio β_{eff}/Λ, and the reactivity using the Inhour equation are proposed.

The purposes of this paper are to give a brief description of the experimental work performed at the IPEN/MB-01 facility related to the experimental determination of the effective delayed neutron parameters and reactivity and to present the process of evaluation of these very important integral responses published in the *International Handbook of Reactor Physics Benchmark Experiments*[24] (IRPhEP Handbook). Also, regarding a very important integral reactor response, the reactivity will be of major concern, and some benchmark values employing the Inhour equation with benchmark values of effective delayed neutron parameters will be proposed. Finally, the accuracy of recently released nuclear data libraries in predicting effective delayed neutron parameters as well as reactivities based on the Inhour equation will be the object of validation and verification. The recently released MCNP6 computer code[39] will be employed to transform the nuclear data in the basic nuclear data libraries into effective delayed neutron parameters adopting the benchmark model of the IPEN/MB-01 reactor. The complete details of the experimental techniques can be found in Refs. 11 through 14, and the

evaluation of these very important integral parameters can be found in Ref. 40.

II. OVERVIEW OF THE MACROSCOPIC AND MICROSCOPIC NOISE EXPERIMENTS

The purpose of the macroscopic noise experiments was to resolve the low-frequency range (< 1.0 Hz) of the auto-power spectral density (APSD) and cross-power spectral density (CPSD). This new in-pile experiment is based on measuring the fluctuations of the neutron population.[41,42] Although this technique is well known[41,42] and well established for many types of measurements,[43–45] there was nothing in the literature regarding experiments involving the determination of the decay constants and/or abundances of delayed neutrons based on this technique. The electronic noise contamination[46] in this very low-frequency region was responsible for the lack of this type of experiment. The experiments performed at the IPEN/MB-01 facility show that it was possible to resolve the low-frequency region; it is possible to extract very useful information from the experiments. In this technique, the APSDs and the CPSD of the signals from two gamma-compensated ionization chambers are measured in a very low-frequency range, and the result is least-squares fitted assuming a point-kinetics model with a delayed neutron precursor six-group structure. The parameters to be fitted are either β_i or λ_I, where β_i and λ_i represent the fraction and decay constant of the delayed neutron group i. To follow the criteria used in the evaluation published in the IRPhEP Handbook,[40] only the results for delayed neutron fraction β_i parameters are presented. The β_{eff}'s obtained as the sum of the partial β's and the relative abundances of delayed neutrons (β_i/β_{eff}) are thus obtained as a by-product. This technique is interesting because it does not perturb the reactor, which is always maintained in a critical state, and so, there is neither contamination of the results due to the harmonic excitation nor residual multiplication, and it seems to not depend on the efficiency and positioning of the detectors.

The purpose of the microscopic noise experiments[13,14] was to measure the effective delayed neutron fraction β_{eff}, Λ, and their ratio β_{eff}/Λ in a purely experimental way, eliminating all parameters that are difficult to measure or calculate. Consequently, the uncertainties associated with these parameters are eliminated, and the accuracy in β_{eff} and in the other kinetic parameters is improved. The experimental methodology employed combines the well-known microscopic noise analysis techniques, Rossi-α and Feynman-α. The ratio β_{eff}/Λ was obtained by extrapolating the curve prompt decay constant α versus the inverse of the detector counting to zero. β_{eff} was obtained by fitting the same curve but considering a very large range of subcritical reactivity. The two-region model curve was adopted for this purpose. The pulse train–recorded time series data were the basic experimental data. The same data set was processed in order to obtain the Rossi-α and Feynman-α distributions.

III. CORE CONFIGURATIONS AND MEASUREMENT PROCEDURES

The experiments employed the standard 28×26 fuel rod configuration as shown in Fig. 1. All geometric data are described in Sec. 1.2 of LEU-COMP-THERM-077 (Ref. 47); however, the set of measurements shown here had no baffle plates surrounding the core. Two banks of control rods control the IPEN/MB-01 reactor. They are located diagonally opposite each other in the core. The A and B symbols in Fig. 1 refer to the two control bank locations, while the S symbol refers to the locations of the two safety rod banks. The safety rod banks were always kept at their fully withdrawn position during the whole set of experiments. Consequently, they do not interfere with the measurements performed for this evaluation. The A and B symbols shown in Fig. 1 refer, respectively, to control banks BC1 and BC2. In all critical configurations, BC1 was always kept at some specific position, and fine criticality control was achieved by the automatic control system continuously positioning BC2 around the true critical position. The control bank position of BC2 is one of the most important parameters for the whole set of experiments of this evaluation.

The control bank system of the IPEN/MB-01 reactor can be considered a high-resolution system, and its linearity has been demonstrated routinely since reactor start-up. The zero of the relative control system (0% withdrawn position) occurs when the bottom of the absorber rods (excluding the bottom plugs) is aligned with the bottom of the fuel region. This reference level or zero was calibrated by a mechanical pattern that allows an accuracy of 0.1 mm. The outermost control bank position (100% withdrawn position) is located 54.6 cm from the bottom of the fuel active length.

Additional information regarding the IPEN/MB-01 reactor and facility is available in benchmark reports LEU-COMP-THERM-077 (Ref. 47) and LEU-COMP-THERM-082 (Ref. 48). This information is not repeated herein but is utilized as reference experimental data and for evaluation of the benchmark experiments.

III.A. Core Configuration and Measurement Procedure for the Macroscopic Noise

The IPEN/MB-01 core configuration considered for the macroscopic noise experiment is shown in Fig. 1. Figure 2 shows the axial view of the positioning of the detectors.

The experiment was performed with the reactor as close to the critical condition as possible at a thermal power of 4.0 W. The complete details of this experiment can be found in Refs. 11 and 12. Here, only the final

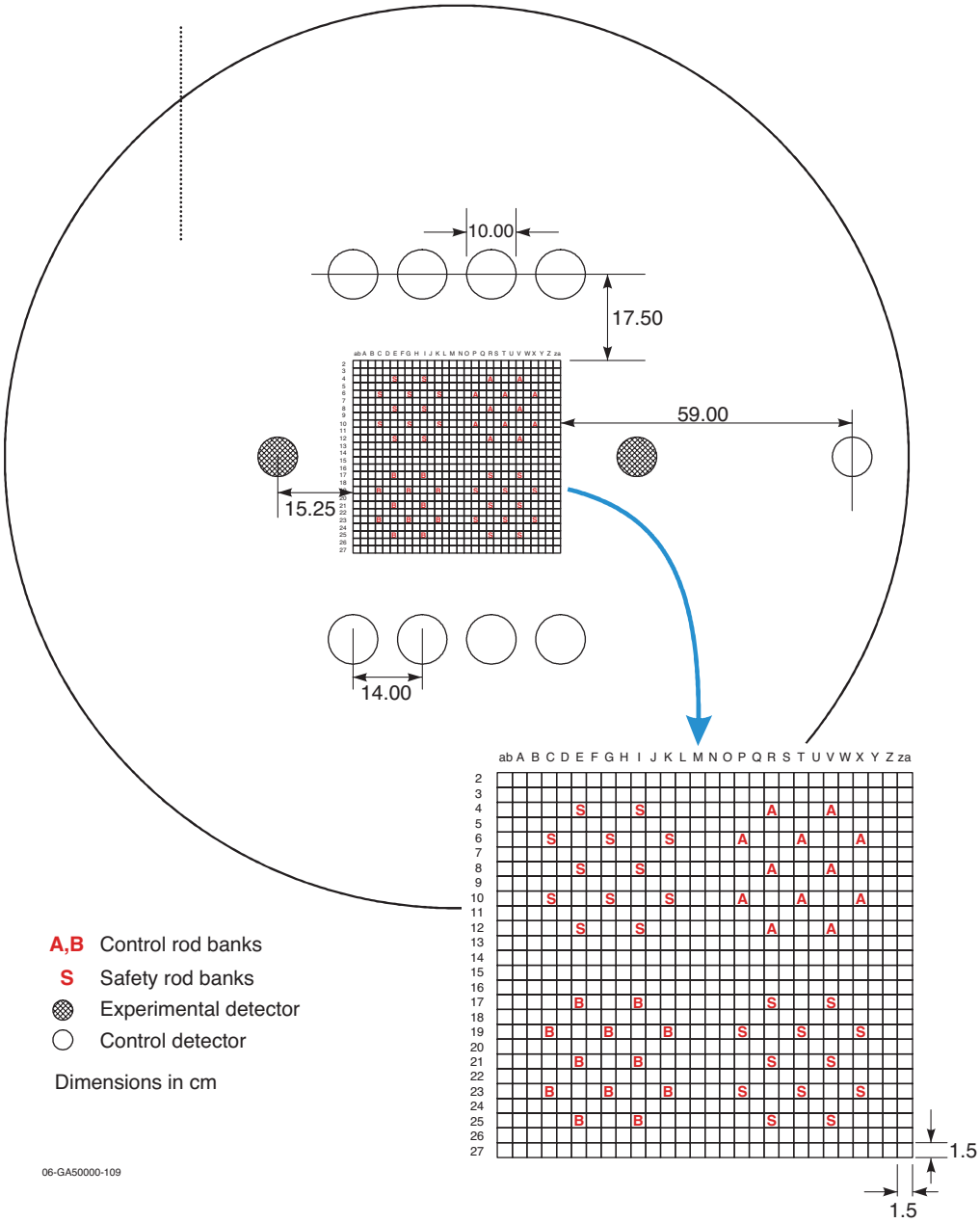

Fig. 1. Schematic diagram of the moderator tank (plan view) showing the detector distribution around the core.

results will be shown. As an example of the experimental data, Fig. 3 shows the CPSD measured data.

We must mention that the low-frequency cutoff of 0.001 Hz of the filter amplifiers employed in the measurements is a limiting factor for this kind of experiment. For example, in the 0- to 3.125-Hz band with 1600 lines of resolution, the first experimental point occurs at $\sim$1.95 mHz, the second point is at 3.91 mHz, and the third point is at 5.86 mHz. However, only the third point is trustworthy; the first two points present some distortion because the cutoff of the filters is not sharp. Thus, there are only four points before the frequency associated with the first decay constant. This will impose some restriction on the first parameter β_1 to be fitted. The acquisition time in the frequency interval ranging from 0.001 to 3.125 Hz is very large, equal to the number of resolution lines divided by the frequency span (1600/3.125) or 512 s.

III.B. Core Configuration and Measurement Procedure for the Microscopic Noise

Two different core configurations were considered for the microscopic noise experiments. Figure 4 shows the

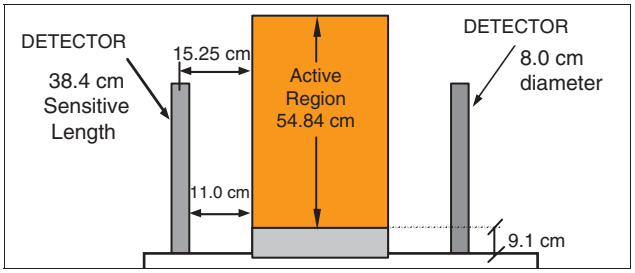

Fig. 2. Side view of the active region and the detector positioning in the west and east faces of the core. (In these conditions, the ionization chambers are in the reflector region ~8.0 cm away from the thermal neutron peak due to the reflector effect.)

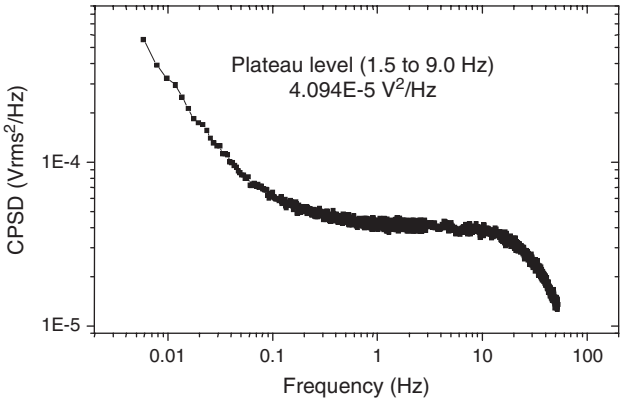

Fig. 3. Absolute value of the measured CPSD with 1000 averages.

x-y cross sections and the detector positions for these configurations.

Figure 4a shows the configuration to obtain β_{eff}/Λ. For this purpose some Rossi-α and Feynman-α distributions were measured near the delayed critical condition. The experimental setup includes one small BF_3 neutron detector of 10-mm diameter and 150-mm height and sensitivity of 2.1 counts per second (cps)/nv placed in the center of the active core. The start-up source (Am-Be, 1Ci) was removed, and the reactor was driven by its own intrinsic source in order to avoid high count rates near the critical state and, consequently, high dead-time losses in the BF_3 detector.

Figure 4b shows the configuration utilized in the experiments to obtain β_{eff}. The prompt neutron generation time Λ and β_{eff}/Λ were obtained indirectly in the experimental procedure. The configuration employed in the experiments was extracted from LEU-COMP-THERM-082 (Ref. 48). Here, eight fuel rods were removed from the standard 28×26 fuel rod configuration, and in their place, eight burnable poison rods were loaded so that the excess reactivity of the core was reduced to nearly zero. Each poison rod is geometrically identical to the fuel rods but is filled with 52 pellets of Al_2O_3-B_4C with 40.53 mg/cm^3 of boron. The details of this configuration as well as a complete description of the materials utilized can be found in Ref. 48. Also, the complete details of the experimental approach adopted to obtain β_{eff}, β_{eff}/Λ, and Λ can be found in Refs. 13 and 14. Here, only the final results and some details of the experiments will be shown.

Considering the control and safety rods fully inserted (Fig. 4b), the subcritical reactivity was approximately −25 000 pcm. In such a way, Rossi-α and Feynman-α distributions can be recorded in a very large range of subcritical reactivity, from nearly −500 to −25 000 pcm. This large subcritical interval leads to a significant variation in the neutron flux and, consequently, in the detector count rate. The detectors employed in the experiment are shown in Table I. They have varying sensitivities and were employed according to the subcritical reactivity level. Also, the start-up source (Am-Be, 1Ci) was inserted in the bottom of the core to drive the system. These actions made possible an accurate measurement of the Rossi-α and Feynman-α distributions in a reasonable length of time. Uncertainty reduction of the α value evaluation and reduction of measurement time for large subcritical levels were attained by a high sensitivity detector, i.e., a ^{3}He neutron detector, whose size and sensitivity were 42 cm in length and 2.6 cm in diameter and 54.3 cps/nv. For measurements at near critical conditions, where the neutron flux is higher, a less sensitive (12.9 cps/nv) boron-lined detector of 10-cm diameter × 33-cm height was used to avoid high count rates and large dead-time effects.

IV. EXPERIMENT RESULTS

IV.A. Macroscopic Noise: Effective Delayed Neutron Parameters

As in Ref. 12, the theoretical APSD for each channel and for the CPSD to be employed in the least-squares approach are thus given, respectively, as

$$\Phi_{kk}(f) = |G(f)|^2 \left(\frac{2N}{\Lambda} D\bar{\nu}\right) \left(\frac{\varepsilon_k q}{\bar{\nu}\Lambda}\right)^2 \left(H_{ek}(f) H_{fk}(f)\right)^2 + \left(H_{ek}(f) H_{fk}(f)\right)^2 2q^2 \varepsilon \frac{N}{\bar{\nu}\Lambda} \quad (1)$$

and

$$\Phi_{kl}(f) = |G(f)|^2 \left(\frac{2N}{\Lambda} D\bar{\nu}\right) \left(\frac{\varepsilon_k \varepsilon_l q^2}{\bar{\nu}^2 \Lambda^2}\right) \times \left(H_{ek}(f) H_{fk}(f)\right) \left(H_{el}(f) H_{fl}(f)\right), \quad (2)$$

where the symbols as well as all the transfer functions are given in Ref. 12.

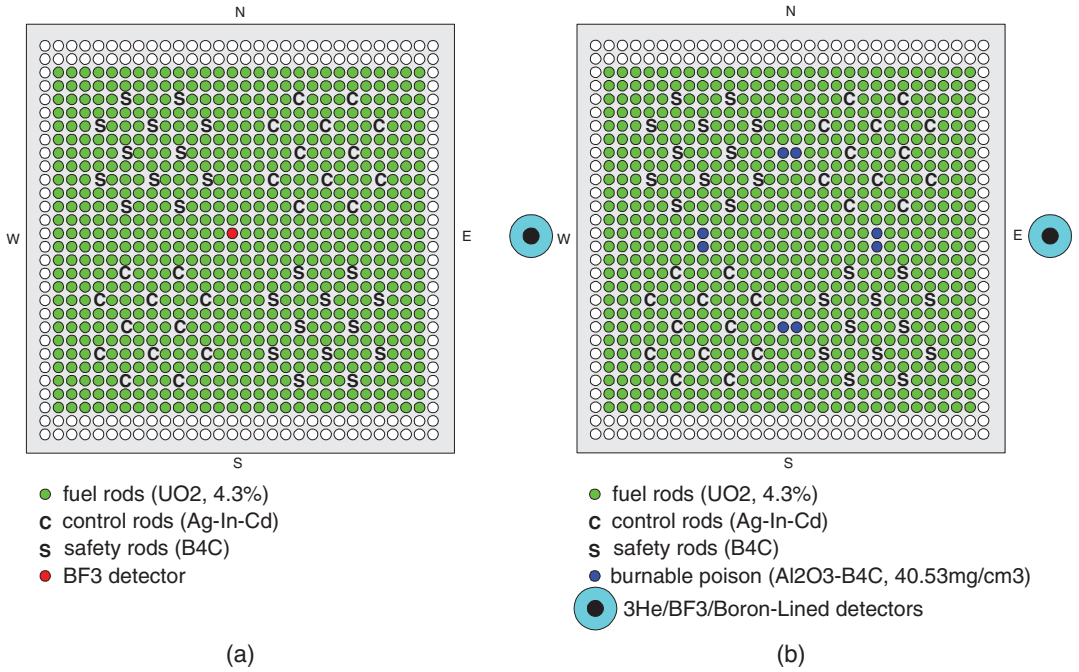

Fig. 4. IPEN/MB-01 core configurations: (a) BF_3 neutron detector positioned in the center of the active core and (b) eight burnable poison rods positioned in the active core and three different detectors in the reflector region.

TABLE I

Pulse-Mode Neutron Detector Specifications

Type	Manufacturer	Model	Operating Voltage (V)	Outside Diameter (mm)	Overall Length (mm)	Sensitivity (cps/nv)
BF_3	Reuter-Stokes	RS-P1-1613-101	2400	25	600	23.1
Boron lined	Centronics	RTC-CPNB35-510	750	77	446	12.9
^3He	Centronics	503He/760/38E	1960	26	420	54.3
Small BF_3	Nuclear Chicago	NC-203	1150	14.7	143	2.1
BF_3	Reuter-Stokes	RS-P1-0836-201	1600	25	800	8.4

The prompt neutron generation time Λ that appears in the reactor transfer function was fixed in all cases at 32 μs based on a series of measurements of β_{eff} and β_{eff}/Λ carried out previously.[49] Convergence of the least-squares approach was not possible when all 12 delayed neutron parameters (β_i and λ_i) were let free. Consequently, the approach adopted in the least-squares method was to fix the decay constants [as given by the most important nuclear data libraries, namely, ENDF/B-VI.8 (Ref. 50), ENDF/B-VI.8 [Los Alamos National Laboratory (LANL) review],[51] and JENDL-3.3 (Ref. 52)] and to fit the abundances. Furthermore, the β_1 parameter must be kept fixed because of the small number of data points below the corresponding frequency of the λ_1 parameter, or ~0.012 Hz. However, there is no serious problem in this in fixing β_1 because there is a linear constraint on β_1, i.e., $\left(\beta_{eff} = \sum_{i=1}^{6} \beta_i\right)$, and there is a gain of one degree of freedom. The least-squares code in all cases employed the standard Levenberg-Marquardt[53] algorithm available in Origin 6.0. In order to get a totally experimental result for β_{eff}, the first decay constant was obtained from an independent measurement. This experiment[54] was in fact done at the IPEN/MB-01 reactor using the Multiple Transient Technique.[10] The λ_1 parameter obtained with the Multiple Transient Technique was $0.012456 \pm 0.000031\ s^{-1}$ and shows excellent agreement with the decay constant of ^{87}Br, the single precursor of the first group.[54]

If the systematic or bias errors are negligible, as seems to be the case here, then the uncertainties in the spectral densities can be obtained following Bendat

and Piersol.[55] The normalized random uncertainties ($\varepsilon = \sigma_\Phi/\Phi$) for each frequency bin of the APSDs is given by

$$\varepsilon(\Phi_{xx}) = \frac{1}{\sqrt{N}} , \quad (3)$$

where N is the number of averages. Note that for the APSDs the error is independent of the frequency. Thus, for $N = 1000$ averages, $\varepsilon(\Phi_{xx}) = 3.2\%$ and each point of the APSD will have an error bar of 3.2% in its magnitude.

The CPSD random uncertainty is frequency dependent, being given by[55]

$$\varepsilon\left(\Phi_{xy}\right) = \frac{1}{\sqrt{\gamma_{xy} N}} , \quad (4)$$

where

γ_{xy} = coherence function $\left(\gamma_{xy} = \dfrac{|\Phi_{xy}|^2}{\Phi_{xx}\,\Phi_{yy}}\right)$

N = number of averages.

It should be noted here that the coherence function in Eq. (4) is the unknown true coherence, and therefore, in the estimate of the random error of the CPSD, the true coherence function must be replaced by the measured function. However, the measured coherence function also has statistical uncertainties that are not considered in the CPSD error estimate, and in such a case, it seems to be adequate to make a conservative analysis of the CPSD error.

This estimate can be made by considering that Eq. (4) has its maximum value of 0.037 (3.7%) at the highest-frequency bin of the CPSD and its minimum value of 0.032 (3.2%) at the lowest-frequency bin of the CPSD. So, an error bar of 3.7% on each point of the CPSD would be reasonable as well as in accordance with a conservative viewpoint.

All uncertainties shown are relative to 1σ. In all cases, the results for each nuclear library for β_{eff} are shown as the arithmetic mean of the fitting parameters obtained from the two APSDs and one CPSD since these spectral densities can be considered as independent measurements. The uncertainties in the final β_{eff} parameters were obtained through the error propagation of a sum of five quantities since β_1 is always kept fixed. Table II shows the final results obtained for the β_{eff} parameter together with the associated experimental uncertainties.

Table II shows that the results for β_{eff} are the same (taking into account the uncertainty of each one) for the decay constants of the three libraries. This is a remarkable result and also shows that fixing β_1 during the least-squares procedure does not represent a serious restriction. From these three results for β_{eff}, one can take the average among them to represent the best value, and that will be the final value of this work. Since the estimate of the correlation coefficient is very difficult in this case, the respective uncertainty is given by the standard error propagation assuming no correlation among the three values of β_{eff}.

TABLE II

Measured β_{eff} from the Macroscopic Noise

Library	β_{eff}
ENDF/B-VI.8	7.47E-03 ± 0.11E-03[a]
ENDF/B-VI.8 (LANL Review)	7.51E-03 ± 0.11E-03
JENDL-3.3	7.47E-03 ± 0.11E-03
Average	7.48E-03 ± 0.07E-03

[a]Read as $7.47 \times 10^{-3} \pm 0.11 \times 10^{-3}$.

In the case of a totally experimental result, as mentioned previously, one can use the first decay constant obtained from an independent experiment[54] carried out at the IPEN/MB-01 reactor. Now, the least-squares procedure is iterative with just the λ_1 parameter fixed and is as follows:

1. Give a reasonable guess for the parameters (β_1, $\beta_2 \ldots \beta_6$) and (λ_2, $\lambda_3 \ldots \lambda_6$), with $\lambda_1 = 0.012456\ s^{-1}$.

2. Initially, λ_1 and β_1 are kept fixed for the fitting of (β_2, $\beta_3 \ldots \beta_6$) or (λ_2, $\lambda_3 \ldots \lambda_6$), iteratively, until no more variations in these parameters occur.

3. The β_1 parameter is now left free for fitting in an iterative process with (β_2, $\beta_3 \ldots \beta_6$) with all decay constants fixed until no more variations among the abundances occur.

4. The β_1 parameter is now left free for fitting in an iterative process with (λ_2, $\lambda_3 \ldots \lambda_6$) with all the abundances fixed until no more variations among the decay constants and the first abundance occur.

5. The last two steps are repeated until no more variations among all the parameters occur.

6. The new sets of (β_1, $\beta_2 \ldots \beta_6$) and (λ_2, $\lambda_3 \ldots \lambda_6$) represent the best fit.

The experimental data were those from the CPSD alone, and the results are shown in Table III. Table III shows that the β_{eff} parameter is totally consistent with the previous results, but its uncertainty of 2.5% is higher than the others because of the utilization of the experimental data of just one spectral density in the fitting procedure. The inclusion of the results of the fitting for the other two APSDs would reduce the uncertainty in the β_{eff} by $\sqrt{3}/3$ or $\sim 58\%$. The β_{eff} uncertainty was calculated assuming no correlation among the individual abundances.

IV.B. Macroscopic Noise: Reactivity Calculations

One of the most important applications of the kinetic parameters is the relation between the reactivity and asymptotic period of a nuclear plant. The Inhour equation gives this relation as

$$\rho_{\$} = \frac{\frac{\Lambda}{T} + \sum_{i=1}^{6} \frac{\beta_i / T}{(1/T) + \lambda_i}}{\sum_{i=1}^{6} \beta_i} , \quad (5)$$

where

T = asymptotic period (s)

$\rho_{\$}$ = reactivity ($).

Using the delayed neutron parameters from Table III and $\Lambda = 32$ μs, the reactivities for some positive and negative periods are shown in Table IV.

The uncertainty in the reactivity calculation was estimated assuming that only β_i and λ_i (except λ_1) present errors and that these parameters are uncorrelated as

$$\sigma_\rho = \sqrt{\left[\left[\frac{-\beta_n \cdot T}{(1+T\cdot\lambda_n)^2 \cdot \beta_{eff}}\right]^2 \cdot (\sigma_{\lambda_n})^2\right] + \sum_{n=1}^{6}\left[\frac{1}{(1+T\cdot\lambda_n)\cdot\beta_{eff}} - \frac{1}{{\beta_{eff}}^2}\cdot\left[\frac{\Lambda}{T} + \sum_{n-1}^{6}\frac{\beta_n}{(1+T\cdot\lambda_n)}\right]\right]^2 \cdot (\sigma_{\beta_n})^2} . \quad (6)$$

IV.C. Microscopic Noise: Effective Delayed Neutron Parameters

The prompt neutron decay constants α for each subcritical measurement were obtained by fitting the Rossi-α and Feynman-α distributions adopting a reflector-core kinetic model.[36] These fitting procedures were performed using the nonlinear weighted least-squares-fitting routine based on the Levenberg-Marquardt algorithm available in Origin 6.0 software (OriginLab Corporation).

According to Ref. 13, the reflector-core Rossi-α distribution obeys the following relationship:

$$p^{c,r}_{Rossi}(\tau) = A^{c,r}\left(N_7^{c,r} e^{\omega_7 \tau} + N_8^{c,r} e^{\omega_8 \tau}\right) + BG , \quad (7)$$

where

$p^{c,r}_{Rossi}(\tau)$ = Rossi-α distribution

τ = elapsed time between two neutron counts

c, r = indices that refer to distributions recorded in the core and reflector region, respectively

A = proportionality constant, with dimension of inverse of time, which relates the adjoint-weighted total number of neutrons to the experimental Rossi-α distributions

BG = term related to the particular solution and experimentally represents the uncorrelated or random component that is added to the solution as a background term

$N_7^{c,r}$, $N_8^{c,r}$ = correlated amplitudes

ω_7, ω_8 = seventh and eighth roots of the reflected-core Inhour equation,[13] and they are given by

TABLE III

Total Experimental Delayed Neutron Parameters of the IPEN/MB-01 Reactor

β_i	λ_i (s^{-1})
(2.679 ± 0.023)E-4[a]	0.012456 (fixed)
(1.463 ± 0.069)E-3	0.0319 ± 0.0032
(1.34 ± 0.13)E-3	0.1085 ± 0.0054
(3.10 ± 0.10)E-3	0.3054 ± 0.0055
(8.31 ± 0.62)E-4	1.085 ± 0.044
(4.99 ± 0.27)E-4	3.14 ± 0.11
β_{eff} = (7.50 ± 0.19)E-3	

[a]Read as $(2.679 \pm 0.023) \times 10^{-4}$.

TABLE IV

Reactivity for Various Periods

T (s)	ρ ($)
1	0.776 ± 0.005
10	0.379 ± 0.007
100	0.092 ± 0.004
200	0.052 ± 0.002
−200	−0.076 ± 0.005
−100	−0.268 ± 0.014
−90	−0.437 ± 0.019
−85	−0.761 ± 0.025

$$\omega_{7,8}=\frac{1}{2\tau_c\tau_r(1-f)}\left\{\begin{array}{l}-\left[(1-\rho)(\tau_c+f\tau_r)+\tau_r(1-f)(\beta_{eff}-\rho)\right]\pm\\ \pm\sqrt{\left\{(1-\rho)(\tau_c+f\tau_r)+\tau_r(1-f)(\beta_{eff}-\rho)\right\}^2-4\tau_c\tau_r(1-f)(1-\rho)(\beta_{eff}-\rho)}\end{array}\right\}, \quad (8)$$

where

τ_c = adjoint-weighted neutron lifetime in the core region

τ_r = adjoint-weighted neutron lifetime in the reflector region

f = fraction of core neutrons returned to the core after having leaked into the reflector

ρ = subcritical reactivity.

The positive and negative signs go with ω_7 and ω_8, respectively. For $\rho < 0$, both roots are negative. Equation (8) shows clearly that the relationship between the decay modes, driven by ω_7 and ω_8, and reactivity are not linear.

The Feynman-α distribution in the reflector-core model obeys Eq. (9) (Ref. 14):

$$Y=\frac{\overline{C^2}-\overline{C}^2}{\overline{C}}-1=-2A^{c,r}\left[\frac{N_7^{c,r}}{\omega_7}\left(1+\frac{1-e^{\omega_7 T}}{\omega_7 T}\right)+\frac{N_8^{c,r}}{\omega_8}\left(1+\frac{1-e^{\omega_8 T}}{\omega_8 T}\right)\right], \quad (9)$$

where

Y = reflected-core Feynman-α distribution

T = time interval to collect the counts

C = detector countings.

Table V shows the measurements of the prompt neutron decay constant α in a very large range of subcritical reactivity. The prompt neutron decay constant α shown in

TABLE V

Final Values and Uncertainties of α

Run	Detector Location	Detector	Average Count Rate (cps)	Control and Safety Rod Positions (%)	α (s^{-1}) (Rossi-α Method)	α (s^{-1}) (Feynman-α Method)
1	Core	Small BF_3	2783.6 ± 194.8	BC1 = 61.89[a]	−241.20 ± 1.28	−240.68 ± 0.54
2	Core	Small BF_3	1441.1 ± 100.9	BC1 = 61.86[a]	−244.89 ± 1.47	−244.83 ± 0.21
3	Core	Small BF_3	889.4 ± 62.3	BC1 = 61.84[a]	−253.19 ± 1.57	−251.47 ± 0.23
4	Reflector	Boron lined	12203.44 ± 1159.81	95.00	[b]	−286.46 ± 1.80
5	Reflector	Boron lined	5016.17 ± 554.81	90.00	−384.64 ± 1.71	−368.30 ± 0.55
6	Reflector	Boron lined	2921.58 ± 293.12	85.00	−491.82 ± 3.14	−464.13 ± 0.53
7	Reflector	Boron lined	2003.12 ± 180.86	80.00	−612.92 ± 3.46	−613.30 ± 2.05
8	Reflector	Boron lined	1502.86 ± 123.03	75.00	−757.86 ± 5.93	−784.33 ± 2.64
9	Reflector	Boron lined	1192.12 ± 93.65	70.00	−934.29 ± 7.07	−1003.26 ± 4.32
10	Reflector	BF_3	3627.72 ± 326.31	65.00	−1194.45 ± 9.69	−1187.30 ± 1.15
11	Reflector	BF_3	3102.90 ± 269.15	60.00	−1481.52 ± 11.29	−1435.34 ± 1.81
12	Reflector	BF_3	2665.45 ± 215.10	55.00	−1697.59 ± 9.73	−1720.08 ± 4.41
13	Reflector	BF_3	2312.98 ± 179.59	50.00	−1960.66 ± 13.58	−2011.75 ± 8.05
14	Reflector	BF_3	2007.94 ± 151.51	45.00	−2200.22 ± 43.34	−2267.90 ± 18.29
15	Reflector	BF_3	1769.32 ± 131.25	40.00	−2445.07 ± 31.17	−2503.92 ± 22.11
16	Reflector	BF_3	1572.82 ± 115.56	35.00	−2755.84 ± 78.05	−2802.28 ± 29.58
17	Reflector	BF_3	1422.63 ± 103.64	30.00	−3033.82 ± 72.79	−3020.27 ± 47.37
18	Reflector	BF_3	1276.53 ± 93.15	25.00	−3234.22 ± 92.24	−3235.43 ± 52.35
19	Reflector	BF_3	1151.62 ± 81.39	20.00	−3491.58 ± 219.62	−3522.26 ± 17.60
20	Reflector	BF_3	1043.56 ± 74.82	15.00	−3663.46 ± 248.92	−3698.16 ± 18.42
21	Reflector	BF_3	953.14 ± 68.66	10.00	−3840.30 ± 290.75	−3944.84 ± 25.07
22	Reflector	BF_3	883.93 ± 62.34	5.00	−3940.13 ± 343.28	−3980.47 ± 34.64
23	Reflector	^3He	382.77 ± 37.67	0	−3998.45 ± 401.24	−4017.11 ± 135.18

[a]Safety banks completely withdrawn (135% withdrawn position) and BC2 at 59.00% withdrawn position.
[b]The low signal-to-noise ratio of the Rossi-α distribution prevented a precise determination of α.

Table V is the seventh (ω_7) root of the reflected-core model Inhour equation in a six-group structure of delayed neutrons. The reason is that near the delayed critical, the seventh root of the reflected-core Inhour equation follows a well-known linear function with the reactivity:

$$\omega_7 = \frac{\rho - \beta_{eff}}{\Lambda} \ . \qquad (10)$$

Assuming that the number of coincidence counts given by the amplitude of the Rossi-α distribution approximately follows a Poisson distribution, its standard deviation σ_{Rossi} is (Ref. 56)

$$\sigma_{Rossi} = \sqrt{p^{c,r}_{Rossi}(t)} \ . \qquad (11)$$

The ratio β_{eff}/Λ was measured from runs 1, 2, and 3. The measurements were performed with the core system driven by its intrinsic source and different control rod positions. Because of the small source strength of the intrinsic source, it was possible to achieve subcritical levels close to the critical state with a reasonable count rate in the BF_3 detector. In this way, the accuracy in a linear extrapolation to the critical condition was improved.

The subcritical reactivity ρ in Eq. (8) was estimated by the Neutron Source Multiplication Method[57,58] (NSMM). In NSMM, it is assumed that the subcritical reactivity ρ is related to the neutron count rate C as $\rho = \varepsilon S/C$ for $\varepsilon S/C >> 1$. This condition is easily met when the reactor is very close to the critical state. Monitoring the count rate C, one can evaluate the deviation of the actual reactivity from the reference reactivity, and when the reactor gets critical, ρ tends to zero, and so does $1/C$. Figure 5 shows the fitted α values obtained from the Rossi-α curves versus the inverse count rates of the BF_3 detector used to perform the measurements (see Table V). The ratio β_{eff}/Λ was obtained extrapolating $(1/C)$ to zero. A linear extrapolation was employed because close to the critical condition, the relation between the decay mode α and reactivity is linear as given by Eq. (10).

The error bars shown in Fig. 5 take into account the uncertainty in the parameter α as well as in the detector count rate. This is accomplished as[59]

$$\sigma_\alpha = \sqrt{\sigma^2_{\alpha_0} + \left[\frac{d\alpha}{d(1/C)}\right]^2 \sigma^2_{1/C}} \ , \qquad (12)$$

where

σ_{α_0} = uncertainty in α given in Table V

$\sigma_{1/C}$ = uncertainty in the inverse count rate

$d\alpha/d(1/C)$ = estimate of the partial derivative of α with respect to the inverse count rate.

In the present study, the derivative $d\alpha/d(1/C)$ was calculated numerically from the α versus $1/C$ curve.

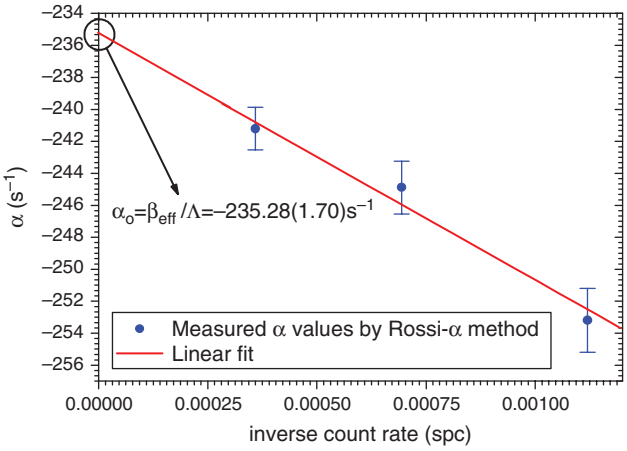

Fig. 5. Plot of the α values given by the Rossi-α method versus the inverse count rate. A linear extrapolation to the critical condition (red line), which is equivalent to $1/C = 0$, gave β_{eff}/Λ of the system as 235.28 ± 1.70 s^{-1}.

The uncertainties $\sigma_{1/C}$ were obtained as follows:

$$\sigma_{(1/C)} = \frac{\sigma_C}{C^2} \ , \qquad (13)$$

where σ_C is the deviation in the detector count rate.

The Feynman-α results follow basically the same procedure. The standard deviation σ_Y of the Y value can be approximately derived from those of the sample variance and mean of the normal distribution[56]:

$$\sigma_Y = \frac{1+Y}{\sqrt{N}} \sqrt{\frac{1+Y}{\bar{c}} + 2} \ , \qquad (14)$$

where N is the number of samples (i.e., the number of counts) for a given time gate T.

The final results for β_{eff}/Λ are shown in Table VI.

The experimental methodology to obtain β_{eff} is based on the reflected-core kinetic model, which relies on the measurements of Rossi-α and Feynman-α distributions at several subcritical levels. The basic experimental data are shown in Table V. Regarding only measurements performed in the reflector region, i.e., runs 4 through 23, Fig. 6 shows the measured α values obtained from the Rossi-α method versus the inverse count rate.

TABLE VI

β_{eff}/Λ Based on Rossi-α and Feynman-α Measurements in the Core Region

	Rossi-α (s^{-1})	Feynman-α (s^{-1})
$\alpha_0 = \beta_{eff}/\Lambda$ (core measurements)	−235.28 (1.70)	−235.57 (0.66)

The Feynman-α method follows basically the same procedure as shown for the Rossi-α method, and only its final results are given. The inverse count rate measurements were conducted with the BF_3 neutron detector RS-P1-0836-201 positioned in the same place where the α values were obtained and at the same control and safety rod positions.

As mentioned, it was recognized that the variation of α with $1/C$ is not linear but shows a behavior described by Eq. (8). Figure 6 shows that there is a stabilization of the prompt decay constant ω_7 for large subcritical reactivities as predicted by the reflected-core kinetic model. This plateau value is according to the reflected-core kinetic model equal to the reflector decay constant λ_r, which corresponds to the inverse neutron lifetime in the reflector $1/\tau_r$. The curve presented in Fig. 6 is bounded asymptotically by Eq. (10) in the vicinity of delayed critical and by $-1/\tau_r$ at deeply subcritical levels.

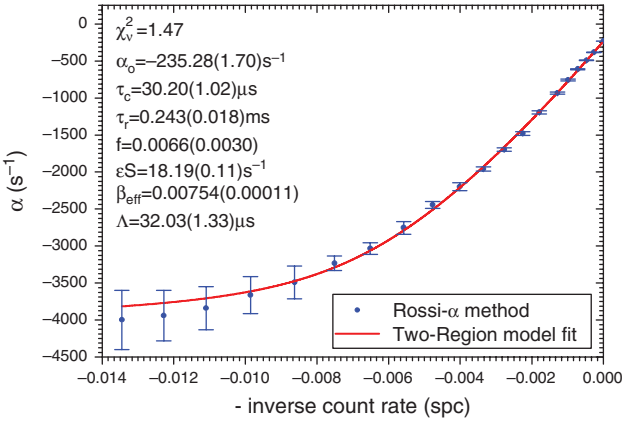

Fig. 6. The prompt neutron decay constant α given by the Rossi-α method versus the inverse count rate.

The parameters τ_c, τ_r, f, and β_{eff} were obtained by fitting the measured α versus the inverse count rate curve using Eq. (8) for ω_7. To this end, a typical weighted least-squares-fitting code, based on the Levenberg-Marquardt algorithm, was developed. The quantity εS was also fitted by replacing the reactivity ρ in Eq. (8) by $\varepsilon S/C$.

Again, here, the uncertainties in the inverse count rates were transferred to the fitted α values using Eq. (12), and the error bars seen in Fig. 6 take into account both contributions.

The fitted curve is indicated by the solid line in Fig. 6, and the fitted parameters are listed in Table VII. The χ^2_ν value showed in Fig. 6 is acceptable, since the error bars in the α parameter near criticality are $<1\%$. Tables VIII and IX show the respective final covariance matrices.

The reflector α_0 value, which is equal to β_{eff}/Λ, was obtained substituting the fitted parameters τ_c, τ_r, f, and β_{eff} in Eq. (8) and calculating for the critical state, i.e., for $\rho = 0.0$. Comparing the data of Tables VI and VII, one may note that the measurements of β_{eff}/Λ both in the core and in the reflector region are consistent.

The prompt neutron generation time Λ can be obtained from the fitted quantities τ_c, τ_r, and f as follows[36]:

$$\Lambda = \frac{1}{1-f}(\tau_c + f\tau_r) \ . \qquad (15)$$

TABLE VII

Evaluation of β_{eff}/Λ, τ_c, τ_r, f, and β_{eff} Based on Rossi-α and Feynman-α Measurements in the Reflector Region

	Rossi-α	Feynman-α
$\alpha_0 = \beta_{eff}/\Lambda$	-234.75 (2.34) s^{-1}	-235.25 (0.96) s^{-1}
τ_c	30.20 (1.02) μs	30.56 (0.48) μs
τ_r	0.243 (0.018) ms	0.232 (0.005) ms
f	0.0066 (0.0030)	0.0055 (0.0012)
β_{eff}	$7.54\ (0.11) \times 10^{-3}$	$7.50\ (0.05) \times 10^{-3}$

TABLE VIII

Covariance Matrix of the Best-Fit Parameters Generated in the Levenberg-Marquardt Algorithm for the Rossi-α Method

	τ_c	τ_r	f	β_{eff}
τ_c	1.0431×10^{-12}	1.5396×10^{-11}	-2.9894×10^{-9}	9.1911×10^{-11}
τ_r	1.5396×10^{-11}	3.3356×10^{-10}	-5.0228×10^{-8}	9.4431×10^{-10}
F	-2.9894×10^{-9}	-5.0228×10^{-8}	9.1677×10^{-6}	-2.1437×10^{-7}
β_{eff}	9.1911×10^{-11}	9.4431×10^{-10}	-2.1437×10^{-7}	1.2719×10^{-8}

TABLE IX

Covariance Matrix of the Best-Fit Parameters Generated in the Levenberg-Marquardt Algorithm for the Feynman-α Method

	τ_c	τ_r	f	β_{eff}
τ_c	2.3452×10^{-13}	2.0615×10^{-12}	-5.6496×10^{-10}	2.3227×10^{-11}
τ_r	2.0615×10^{-12}	2.8073×10^{-11}	-5.9350×10^{-9}	1.4747×10^{-10}
f	-5.6496×10^{-10}	-5.9350×10^{-9}	1.5306×10^{-2}	-4.4100×10^{-8}
β_{eff}	2.3227×10^{-11}	1.4747×10^{-10}	-4.4100×10^{-8}	2.6596×10^{-9}

The final value is $\Lambda = 32.03 \pm 0.37$ μs, which again is consistent with the value given in Table VI.

The uncertainties in the fitted parameters were calculated from the diagonal elements in the covariance matrix. The uncertainty in the quantity α_0, which was derived from the fitted parameters, was obtained using the well-known error propagation formula including the terms containing the off-diagonal elements of the covariance matrix,[58] i.e.,

$$\begin{aligned}\sigma^2_{\alpha_0} = &\left(\frac{\partial\alpha_0}{\partial\tau_c}\right)^2\sigma^2_{\tau_c} + \left(\frac{\partial\alpha_0}{\partial\tau_r}\right)^2\sigma^2_{\tau_r} + \left(\frac{\partial\alpha_0}{\partial f}\right)^2\sigma^2_f \\ &+ \left(\frac{\partial\alpha_0}{\partial\beta_{eff}}\right)^2\sigma^2_{\beta_{eff}} + 2\left(\frac{\partial\alpha_0}{\partial\tau_c}\frac{\partial\alpha_0}{\partial\tau_r}\right)\sigma^2_{\tau_c\tau_r} \\ &+ 2\left(\frac{\partial\alpha_0}{\partial\tau_c}\frac{\partial\alpha_0}{\partial f}\right)\sigma^2_{\tau_c f} + 2\left(\frac{\partial\alpha_0}{\partial\tau_c}\frac{\partial\alpha_0}{\partial\beta_{eff}}\right)\sigma^2_{\tau_c\beta_{eff}} \\ &+ 2\left(\frac{\partial\alpha_0}{\partial\tau_r}\frac{\partial\alpha_0}{\partial f}\right)\sigma^2_{\tau_r f} + 2\left(\frac{\partial\alpha_0}{\partial\tau_r}\frac{\partial\alpha_0}{\partial\beta_{eff}}\right)\sigma^2_{\tau_r\beta_{eff}} \\ &+ 2\left(\frac{\partial\alpha_0}{\partial f}\frac{\partial\alpha_0}{\partial\beta_{eff}}\right)\sigma^2_{f\beta_{eff}}. \end{aligned} \quad (16)$$

The quantities σ^2_{uv} are the covariances between the variables u and v. Both variances σ^2_u and covariances σ^2_{uv}, are obtained from the estimated covariance matrix of the standard errors in the fitted parameters τ_c, τ_r, f, and β_{eff}.

IV.D. The Λ Measurement Methodology

The prompt neutron generation time Λ was obtained in two different ways.

In the first way, Λ can be trivially obtained through the relation

$$\Lambda = \frac{\beta_{eff}}{\left(\beta_{eff}/\Lambda\right)}, \quad (17)$$

where β_{eff} and $\alpha_0 = \beta_{eff}/\Lambda$ are values given in Tables VI and VII, respectively. Table X lists the final results.

TABLE X

Evaluation of Λ Based on Rossi-α and Feynman-α Measurements Using Eq. (17)

	Rossi-α	Feynman-α
Λ (μs)	32.04 (0.52)	31.84 (0.23)

TABLE XI

Evaluation of Λ Based on Rossi-α and Feynman-α Measurements Using Eq. (18)

	Rossi-α	Feynman-α
Λ (μs)	32.03 (0.37)	32.02 (0.22)

The uncertainties in the final values were estimated via the standard error propagation formula.

In the second way, assuming that in most reflected systems the neutron lifetime in the reflector region is sufficiently small, such that $\tau_r\omega_j << 1$, the fitted quantities τ_c, τ_r, and f can be combined to yield the prompt neutron generation time Λ through Eq. (18) (Ref. 35):

$$\Lambda = \frac{1}{1-f}(\tau_c + f\tau_r). \quad (18)$$

The final values are listed in Table XI.

Since Λ is derived from the fitted parameters τ_c, τ_r, and f, its uncertainty is obtained using the well-known error propagation formula including the terms containing the off-diagonal elements of the covariance matrix, i.e.,

$$\begin{aligned}\sigma^2_\Lambda = &\left(\frac{\partial\Lambda}{\partial\tau_c}\right)^2\sigma^2_{\tau_c} + \left(\frac{\partial\Lambda}{\partial\tau_r}\right)^2\sigma^2_{\tau_r} + \left(\frac{\partial\Lambda}{\partial f}\right)^2\sigma^2_f \\ &+ 2\left(\frac{\partial\Lambda}{\partial\tau_c}\frac{\partial\Lambda}{\partial\tau_r}\right)\sigma^2_{\tau_c\tau_r} + 2\left(\frac{\partial\Lambda}{\partial\tau_c}\frac{\partial\Lambda}{\partial f}\right)\sigma^2_{\tau_c f} \\ &+ 2\left(\frac{\partial\Lambda}{\partial\tau_r}\frac{\partial\Lambda}{\partial f}\right)\sigma^2_{\tau_r f}. \end{aligned} \quad (19)$$

The variances σ_u^2 and the covariance σ_{uv}^2 were obtained from the estimated covariance matrix of the standard errors showed in Tables VIII and IX.

The constraint among the fitted parameters τ_c, τ_r, and f described by Eq. (18) brings out an important characteristic to the adopted fitting procedure. It was noted that the fitting procedure is not sensitive enough to determine these parameters separately with certain accuracy. However, Λ can be derived from Eq. (18), with an uncertainty of $\sim 1\%$. The uncertainty in Λ is strongly reduced when the covariance terms are considered in the error propagation formula. Furthermore, a reasonably accurate initial guess for τ_r can be obtained from the asymptote at $-1/\tau_r$ in the α versus inverse count rate curve. In summary, the constraint among τ_c, τ_r, and f and the accurate initial guess for τ_r improve confidence in the prompt neutron generation time Λ.

V. EVALUATION OF RECOMMENDED EXPERIMENTAL DATA

Three independent noise experiments were carried out in order to obtain the effective delayed neutron fraction β_{eff}, the prompt neutron generation time Λ, and the ratio β_{eff}/Λ. Tables XII and XIII summarize the final results for β_{eff} and Λ, respectively. The value of Λ, based on the spectral density measurements shown in Table XIII, was based on a series of macroscopic noise experiments as described in Ref. 49.

The recommended experimental values for β_{eff} and Λ were obtained via the weighted means of data from Tables XII and XIII, respectively. The weighted mean is given by[59]

$$\mu = \frac{\sum x_i/\sigma_i^2}{\sum 1/\sigma_i^2} , \tag{20}$$

where each data point x_i in the sum is weighted inversely by its own variance σ_i^2. The variance of mean is written as

$$\sigma_\mu^2 = \frac{1}{\sum 1/\sigma_i^2} . \tag{21}$$

The recommended experimental values for β_{eff} and Λ given in Tables XII and XIII, respectively, were combined to yield the ratio $\alpha_0 = \beta_{eff}/\Lambda$. The final value is

$$\alpha_0 = \frac{\beta_{eff}}{\Lambda} = \frac{(750 \pm 4) \times 10^{-5}}{(31.96 \pm 0.13) \times 10^{-6}\text{s}} = 234.66 \pm 1.51\ \text{s}^{-1} . \tag{22}$$

The final uncertainty in α_0 was calculated using the standard error propagation formula.

TABLE XII

Evaluation of β_{eff} Based on Reactor Noise Experiments

Method	β_{eff} (pcm)
Rossi-α	754 ± 11
Feynman-α	750 ± 5
Spectral densities, ENDF/B-VI.8	747 ± 13
Spectral densities, ENDF/B-VI.8 (LANL)	751 ± 11
Spectral densities, JENDL 3.3	747 ± 11
	Weighted mean = 750 ± 4

TABLE XIII

Evaluation of Λ Based on Reactor Noise Experiments

Method	Λ (μs)
Rossi-α, Eq. (17)	32.04 ± 0.52
Rossi-α, Eq. (18)	32.03 ± 0.37
Feynman-α, Eq. (17)	31.84 ± 0.23
Feynman-α, Eq. (18)	32.02 ± 0.32
Spectral densities[48]	31.99 ± 0.33
	Weighted mean = 31.96 ± 0.13

VI. EFFECT OF PARAMETER UNCERTAINTIES ON β_{eff}, Λ, and β_{eff}/Λ AND ON THE REACTIVITY

The uncertainty due to the geometrical and material composition data was obtained in the companion HAMMER-TECHNION/CITATION codes. The HAMMER-TECHNION code[60] is used for the few-group cross-section generation, and the CITATION diffusion code[60] (a three-dimensional deterministic diffusion theory code) is used for the neutron diffusion into the reactor core. The model included all details of the fuel region, control rods, reflector, etc. The convergence criterion used was 10^{-6}. Since the uncertainties in the majority of cases are rather small, the use of a Monte Carlo approach has been discarded because it would require a very large number of neutron histories to reduce the standard deviation to a level smaller than the uncertainty itself. The approach adopted based on the deterministic code has been found to be adequate. All parameters and the corresponding uncertainties are at 20°C. The uncertainties considered are those arising from the ^{235}U enrichment, UO_2 density, UO_2 pellet diameter, cladding outer and inner diameters, pitch, active core height, cladding density and composition, ^{234}U content, UO_2 stoichiometric factor, water density, bottom alumina height, control rod density, and control rod composition. The effect of the fuel

impurities on the reactivity was estimated to be of the order of 1 pcm, which is negligible for the analysis considered here. The effect of the water impurities is also small (<1 pcm). Neither will be considered further in the analyses.

Results for the CITATION calculations for the experimental configurations are shown in Table XIV for 20°C.

Combining the geometric and material uncertainties from Table XIV and the experimental uncertainties for β_{eff} and Λ given in Tables XII and XIII, respectively, the total uncertainties in these parameters σ_t can be obtained as

$$\sigma_t\left(\beta_{eff}\right) = \sqrt{4^2 + 3.269^2} \cong 5\,\text{pcm} \tag{23}$$

and

$$\sigma_t(\Lambda) = \sqrt{0.13^2 + 1.049^2} \cong 1.06\,\mu\text{s}\,. \tag{24}$$

The total uncertainty in β_{eff}/Λ was calculated following a standard error propagation procedure as

$$\sigma_{\beta_{eff}/\Lambda} = \sqrt{\left(\frac{\partial(\beta_{eff}/\Lambda)}{\partial\Lambda}\right)^2 \sigma_\Lambda^2 + \left(\frac{\partial(\beta_{eff}/\Lambda)}{\partial\beta_{eff}}\right)^2 \sigma_{\beta_{eff}}^2} \cong 7.92\,\text{s}^{-1}\,, \tag{25}$$

where the total uncertainties for β_{eff} and Λ are given by Eqs. (23) and (24), respectively.

The impact of the geometric and material uncertainties for the determination of the reactivities using the

TABLE XIV

CITATION Calculations of the Geometrical and Material Composition Uncertainties for 20°C

Parameter	Parameter Value $\pm 1\sigma$	$\Delta\beta_{eff}$		$\Delta\beta_{eff}$ Uncertainty (pcm)	Λ		$\Delta\Lambda$ Uncertainty (μs)
		$+1\sigma$ (pcm)	-1σ (pcm)		$+1\sigma$ (μs)	-1σ (μs)	
^{235}U enrichment (%)	4.3486 ± 0.0021	0.004	0.008	0.008	0.007	0.007	0.007
UO_2 density (g/cm^3)	10.1771 ± 0.1018	0.050	0.048	0.050	0.183	0.186	0.186
UO_2 pellet diameter (mm)	8.4894 ± 0.00475	0.001	0.002	0.002	0.002	0.002	0.002
Cladding outer diameter (mm)	9.8074 ± 0.0169	0.061	0.066	0.066	0.033	0.033	0.033
Cladding inner diameter (mm)	8.5746 ± 0.0243	0.062	0.054	0.062	0.022	0.051	0.051
Pitch (mm)	15.000 ± 0.392	3.010	3.256	3.256	1.024	0.956	1.024
Active core height (cm)	54.84 ± 0.3544	0.275	0.081	0.275	0.118	0.119	0.119
Cladding density (g/cm^3)	7.9207 ± 0.0005	0	0	0	0	0	0
^{55}Mn in cladding stainless steel (wt%)	1.6867 ± 0.11015	0.006	0.002	0.006	0.011	0.010	0.011
Cladding composition	Ni = 10.0433 ± 0.125 Cr = 18.34 ± 0.2163 Co = 0.215 ± 0.00707 Mo = 0.17 ± 0.01414	0.005	0.001	0.005	0.002	0.002	0.002
^{234}U (wt%)	0.034 ± 0.000034	0.014	0.019	0.019	0.005	0.005	0.005
UO_2 stoichiometric factor (%)	88.125 ± 0.023	0.009	0.008	0.009	0.004	0.004	0.004
Water density (g/cm^3)	0.99820 ± 0.00002 (Ref. 67)	0	0	0	0	0	0
Bottom alumina height (mm)	90.28 ± 0.09	0	0	0	0	0	0
Control rod density	10.007 ± 0.004	0	0	0	0	0	0
Control rod composition	Ag = 0.7934 ± 0.0015 In = 0.1496 ± 0.0014 Cd = 0.0483 ± 0.001	0	0	0	0	0	0
Total[a]	—	—	—	3.269	—	—	1.049

[a]Total uncertainty is equal to $\sqrt{\sum\left(\Delta\beta_{eff}\right)^2}$ or $\sqrt{\sum(\Delta\Lambda)^2}$.

Inhour equation with the totally experimental parameters given in Table III was negligible ($\rho < 1.0$ pcm) compared to the experimental uncertainties. The relative abundances of delayed neutrons (β_i/β_{eff}) shows very little sensitivity to geometrical and material data of the facility, and the reactivity shows very little sensitivity to the value of β_{eff}/Λ. Therefore, only the experimental uncertainties are used in this case.

VII. BENCHMARK MODEL SPECIFICATIONS FOR KINETIC MEASUREMENTS

The complete details of the benchmark model including geometric and material data can be found in the IRPhEP Handbook. Here, only some highlights will be shown.

The benchmark geometric model at 20°C for the IPEN/MB-01 configuration is based on the rectangular (28×26) configuration with the control banks inserted to the critical condition. The benchmark model basically follows the same pattern as in LEU-COMP-THERM-077. All material and geometrical data at 20°C are given in Sec. 1 of LEU-COMP-THERM-077. The as-built data are judged to be more realistic and precise for the benchmark specification. The simplifications in the model were discussed to some extent in this evaluation and also in LEU-COMP-THERM-082. The impact of these simplifications in the effective delayed neutron parameters is minimal, and consequently, the proposed benchmark model fully represents the IPEN/MB-01 core. The temperature to be used in the calculations is 20°C.

VII.A. Experimental and Benchmark Model Kinetic Parameters and Reactivity Measurements

The benchmark model for the kinetic parameters and their estimated uncertainties (1σ) are given in Table XV. The experimental β_{eff} and Λ values are given in Tables XII and XIII, respectively. Because thermocouples and control and instrumentation tubes are not included in the benchmark model, the total of their measured reactivity effect (-33.5 pcm at 20°C; 12.5 pcm for omitting thermocouples and 21 pcm for omitting tubes of neutron detectors) will not impose any restrictions on the effective kinetic parameters since these parameters are not very sensitive to the reactivity. Combining the geometric and material uncertainties from Table XIV and the experimental uncertainty from Tables XII and XIII, a total uncertainty can be readily obtained. Since the total uncertainty is small and well understood, the proposed experiment is acceptable as a benchmark experiment. Table XV summarizes the benchmark model for β_{eff}, β_{eff}/Λ, and Λ. The benchmark value for the reactivity is given in Table XVI. The uncertainties considered here are the ones arising only from the experiments.

TABLE XV

Benchmark Model for β_{eff}, β_{eff}/Λ, and Λ

β_{eff} (pcm)	β_{eff}/Λ (s^{-1})	Λ (μs)
750 ± 5	234.66 ± 7.92	31.96 ± 1.06

TABLE XVI

Benchmark Model for Reactivity

T (s)	ρ ($)
1	0.776 ± 0.005
10	0.379 ± 0.007
100	0.092 ± 0.004
200	0.052 ± 0.002
−200	−0.076 ± 0.005
−100	−0.268 ± 0.014
−90	−0.437 ± 0.019
−85	−0.761 ± 0.025

The quantities to be calculated are expressed mathematically as

$$\beta_{eff_j} = \frac{1}{F}\int \ldots \int \sum_{i=1}^{N} \chi_{d_j}^{i}(E)\beta_j^i \nu\Sigma_f^i(r,E')\phi(r,\Omega',E')\phi^* \times (r,\Omega,E)drd\Omega' dE' d\Omega dE \,, \quad (26)$$

$$\beta_{eff} = \sum_{i=1}^{6} \beta_{eff_j} \,, \quad (27)$$

$$\Lambda = \frac{1}{F}\iiint \frac{1}{v(E)}\phi^*(r,\Omega,E)\phi(r,\Omega,E)drd\Omega dE \,, \quad (28)$$

$$F = \int \ldots \int \chi(E)\nu\Sigma_f(r,E')\phi(r,\Omega',E')\phi^* \times (r,\Omega,E)drd\Omega' dE' d\Omega dE \,, \quad (29)$$

and

$$\rho_{\$} = \frac{\dfrac{\Lambda}{T} + \displaystyle\sum_{i=1}^{6} \dfrac{\beta_{eff\,i}/T}{(1/T)+\lambda_i}}{\displaystyle\sum_{i=1}^{6} \beta_{eff\,i}} \,, \quad (30)$$

where N is the number of fissile and/or fissionable nuclides, six groups of delayed neutrons has been assumed, and all other symbols follow the same meaning as in Bell and Glasstone.[62]

VIII. COMPARISON THEORY/EXPERIMENT

The effective delayed neutron parameters were calculated with MCNP6. This last version of MCNP incorporates, among several other improvements, the determination of the adjoint fluxes that make the determination of the effective delayed neutron parameters more consistent and precise. The theoretical values were calculated by MCNP6 adopting the benchmark model of the IPEN/MB-01 reactor as described in the IRPhEP Handbook. Geometric and material data of the IPEN/MB-01 reactor model were also taken from the IRPhEP Handbook. The nuclear data libraries considered in this work are ENDF/B-VII.0 (Ref. 63), ENDF/B-VII.1 (Ref. 64), JEFF-3.1.1 (Ref. 65), JENDL-3.3 (Ref. 53), and JENDL-4.0 (Ref. 66). The theory/experiment comparison is shown in terms of (C − E)/E given in units of percent, where C represents the calculated value and E represents the benchmark model values. The uncertainties in the (C − E)/E values include the benchmark value uncertainties and the statistical uncertainty in the calculated values arising from the Monte Carlo method.

A comparison of the theoretical values of β_{eff}, β_{eff}/Λ, and Λ to the benchmark model value is shown in Table XVII. Also shown in Table XVII is the comparison of λ_1, the decay constant of the first group of delayed neutrons. It will be shown shortly that this decay constant has an important bearing in the determination of the reactivity for negative periods. Table XVII shows clearly that all nuclear data libraries considered in this work meet the recommended accuracy for β_{eff} calculations ($|C-E|/E < 3\%$). The highest discrepancy occurs for JEFF-3.1.1, although its value is inside the 3σ uncertainty range of the benchmark value. The calculated values of β_{eff}/Λ and the prompt neutron generation time Λ for all nuclear data libraries studied in this work show excellent performance. All the calculated values of β_{eff}/Λ and the prompt neutron generation time Λ are inside the 3σ uncertainty range of the benchmark value, although the highest discrepancy occurs for JEFF-3.1.1. The calculated prompt neutron generation time shows very little sensitivity to the nuclear data library employed in the calculations. In a general sense when compared to the benchmark value (31.96 ± 1.06 μs), it shows a systematic underprediction of $\sim 4\%$.

The first decay constant differs significantly only for ENDF/B-VII.1. All other nuclear data libraries show λ_1 very close to the experimental value. The experimental value is 0.012456 ± 0.000031.

Table XVIII compares the reactivity using the Inhour equation predicted by ENDF/B-VII.0 and ENDF/B-VII.1, while Table XIX shows the same comparison for JEFF-3.1.1, JENDL-3.3, and JENDL-4.0. In contrast to the comparison made in Table XVII, here the discrepancies are more severe, and there is a clear tendency to increase the deviation with the absolute value of the reactivity for negative periods. Table XVIII shows that neither ENDF/B-VII.0 nor ENDF/B-VII.1 produces satisfactory results for negative periods less than -100 s. For positive periods the agreement between theory and experiment of these two nuclear data libraries is very good. However, for negative periods less than -100 s, the reactivities predicted by these libraries are well beyond the 3σ range of the benchmark uncertainty. For ENDF/B-VII.1, the main cause is its decay constant λ_1 of the first delayed neutron group, which is a bit overestimated. In order to show the sensitivity of the reactivity to the first decay constant, Table XVIII shows the ENDF/B-VII.1 results when this first decay constant is replaced by the experimental value. The agreement now is significantly improved with almost all values falling inside the 3σ range of the benchmark uncertainty. The remaining discrepancy may be attributed to the effective delayed neutron abundances of ^{235}U and ^{238}U and to the remaining delayed neutron decay constants.

Contrary to the performance of the ENDF/B-VII.0 and ENDF/B-VII.1 libraries, the JEFF-3.1.1, JENDL-3.3, and JENDL-4.0 libraries show excellent performance in the determination of reactivities. The comparison is shown in Table XIX. JEFF-3.1.1 and JENDL-3.3 show all their results inside the 3σ range of the benchmark uncertainty. JENDL-4.0 shows some discrepancy for a period of -85 s. The other results are satisfactory considering the uncertainty of the benchmark value.

TABLE XVII

Comparison of the Calculated β_{eff}, β_{eff}/Λ, and Λ to the Benchmark Value

	ENDF/B-VII.0 (C − E)/E (%)	ENDF/B-VII.1 (C − E)/E (%)	JEFF-3.1.1 (C − E)/E (%)	JENDL-3.3 (C − E)/E (%)	JENDL-4.0 (C − E)/E (%)
β_{eff}	0.00 ± 0.82	-0.53 ± 0.94	2.13 ± 0.95	-0.55 ± 0.94	-0.67 ± 0.94
β_{eff}/Λ	4.11 ± 3.54	3.41 ± 4.86	6.42 ± 4.93	3.25 ± 4.85	3.24 ± 4.85
Λ	-3.89 ± 3.19	-3.78 ± 4.60	-4.00 ± 4.60	-4.00 ± 4.60	-3.76 ± 4.60
λ_1 (s^{-1})[a]	0.01249	0.01335	0.01247	0.01244	0.01248

[a]The experimental value is 0.012456 ± 0.000031.

TABLE XVIII

Comparison Theory/Experiment for the Reactivities Inferred from the Inhour Equation of ENDF/B-VII.0 and ENDF/B-VII.1

Period (s)	ENDF/B-VII.0 (C−E)/E (%)	ENDF/B-VII.1 (C−E)/E (%)	ENDF/B-VII.1 (C−E)/E (%)[a]
1	−3.75 ± 0.82	−2.05 ± 0.68	−2.04 ± 0.68
10	−9.01 ± 1.83	−7.05 ± 2.00	−6.99 ± 1.83
100	−12.80 ± 4.26	−10.40 ± 4.02	−9.80 ± 4.05
200	−13.23 ± 4.59	−10.94 ± 3.59	−10.08 ± 3.63
−200	−14.51 ± 5.96	−13.68 ± 5.79	−10.66 ± 6.01
−100	−16.35 ± 4.78	−23.77 ± 4.27	−10.74 ± 5.10
−90	−17.76 ± 4.29	−34.86 ± 3.22	−10.59 ± 4.64
−85	−20.03 ± 3.79	−50.89 ± 2.07	−10.41 ± 4.18

[a]The experimental value 0.012456 ± 0.000031 s^{-1} replaces λ_1.

TABLE XIX

Comparison Theory/Experiment for the Reactivities Inferred from the Inhour Equation of JEFF-3.1.1, JENDL-3.3, and JENDL-4.0

Period (s)	JEFF-3.1.1 (C−E)/E (%)	JENDL-3.3 (C−E)/E (%)	JENDL-4.0 (C−E)/E (%)
1	1.15 ± 0.69	1.36 ± 0.67	1.62 ± 0.67
10	3.14 ± 2.00	3.28 ± 1.92	2.88 ± 1.94
100	4.32 ± 4.66	4.60 ± 4.61	2.69 ± 4.56
200	4.24 ± 4.17	4.61 ± 4.12	2.37 ± 4.07
−200	2.71 ± 6.87	3.58 ± 6.88	0.03 ± 6.67
−100	−2.88 ± 5.45	−0.35 ± 5.56	−6.1 ± 5.30
−90	−6.91 ± 4.71	−2.82 ± 4.89	−9.9 ± 4.64
−85	−11.24 ± 4.05	−4.64 ± 4.31	−16.8 ± 4.03

IX. CONCLUSIONS

The evaluation of the experiments for determining the effective delayed neutron parameters and reactivity using the Inhour equation has been successfully accomplished. The evaluated data are of very good quality, fulfilling the requirements of a benchmark.

The macroscopic (low-frequency range) and microscopic (Rossi-α and Feynman-α) noise experiments performed at the IPEN/MB-01 facility show that it was possible not only to resolve the low-frequency region but also to extract very useful information. The experimental procedures did not require any correction factor or other experimental results, and the least-squares procedure adopted allowed very accurate precise predictions of the effective delayed neutron parameters, like β_{eff}, to be extracted. All three experiments produced consistent results for the effective delayed neutron parameters. Particularly, the macroscopic noise experiment was able to resolve the low-requency range and from the raw experimental data to extract the relative abundance of delayed neutrons employing a least-squares approach. On the other hand, the observation of two decay modes in the Rossi-α distributions recorded in the reflector region and the nonlinear behavior between prompt neutron decay constant α and the inverse count rate demonstrated that the kinetic behavior of the IPEN/MB-01 core is governed by the two-region model. Furthermore, the prompt neutron generation time Λ was also measured in a purely experimental way.

The delayed neutron data of the recently released nuclear data libraries ENDF/B-VII.1, JENDL-4.0, and JEFF-3.1.1 as well as ENDF/B-VII.0 and JENDL-3.3 have been the object of analysis. The recently released MCNP6 has been employed to transform the delayed neutron data of these nuclear data libraries into effective delayed neutron parameters adopting the benchmark model of the IPEN/MB-01 reactor available in the IRPhEP Handbook. The analysis reveals that all these nuclear data libraries produced satisfactory results for β_{eff}, β_{eff}/Λ, and Λ. The same cannot be said for the determination of the reactivity employing the Inhour

equation. It was shown that there is a clear tendency to increase the deviation with the absolute value of the reactivity for negative periods. Only JENDL-3.3 and JEFF-3.1.1 produced results that are inside the 3σ range of the benchmark uncertainty. Specifically for the case of ENDF/B-VII.1, a good part of the discrepancy is due to the decay constant of the first group of delayed neutrons. This decay constant is overestimated according to the experimental value measured in the IPEN/MB-01 reactor.

ACKNOWLEDGMENTS

The authors are grateful to S. C. van der Marck of Nuclear Research and Consultancy Group for providing the MCNP6 output runs of ENDF/B-VII.1, JENDL-4.0, and JEFF-3.1.1 of this work. The authors are also grateful to Fundação de Amparo à Pesquisa do Estado de São Paulo for providing the financial support for this work under research project Nos. 2001/14450-0 and 06/61452-2.

REFERENCES

1. "Cross Section Evaluation Working Group Benchmark Specification," ENDF-202 (BNL-19302), Brookhaven National Laboratory.

2. S. R. BIERMAN, E. D. CLAYTON, and L. E. HANSEN, "Critical Experiments with Homogeneous Mixtures of Plutonium and Uranium Oxides Containing 8, 15, and 30 wt% Plutonium," *Nucl. Sci. Eng.*, **50**, 115 (1973); http://dx.doi.org/10.13182/NSE73-2.

3. J. C. MANARANCHE et al., "Critical Experiments with Lattices of 4.75 wt% ^{235}U-Enriched UO_2 Rods in Water," *Nucl. Sci. Eng.*, **71**, 154 (1979); http://dx.doi.org/10.13182/NSE79-4.

4. J. HARDY, JR., D. KLEIN, and J. J. VOLPE, "A Study of Physics Parameters in Several Water-Moderated Lattices of Slightly Enriched and Natural Uranium," WAPD-TM-931, Bettis Atomic Power Laboratory (Mar. 1970).

5. H. TUSURUTA et al., "Critical Sizes of Light Water Moderated UO_2 and PuO_2-UO_2 Lattices," JAERI-1254, Japan Atomic Energy Research lnstitute (1977).

6. E. JOHANSON, "Data and Results for KRITZ Experiments on Regular H_2O/Fuel Pin Lattices at Temperatures Up to 245°C," STUDSVIK/NS-90/l33, Studsvik Energiteknik AB (1990).

7. C. GOLINELLI et al., "Temperature Coefficient and Doppler Effect Measurements," presented at Topl. Mtg. Advances in Reactor Physics and Shielding, Sun Valley, Idaho, September 14–17, 1980.

8. A. DOS SANTOS et al., "Reactivity Coefficients of IPEN/MB-0l Reactor," *Proc. Int. Conf. Physics of Reactors (PHYSOR-96)*, Mito, Ibaraki, Japan, September 16–20, 1996.

9. G. D. SPRIGGS, "Two Rossi-α Techniques for Measuring the Effective Delayed Neutron Fraction," *Nucl. Sci. Eng.*, **113**, 161 (1993); http://dx.doi.org/10.13182/NSE93-2.

10. G. D. SPRIGGS, "In-Pile Measurement of the Decay Constants and Relative Abundance of Delayed Neutrons," *Nucl. Sci. Eng.*, **114**, 342 (1993); http://dx.doi.org/10.13182/NSE92-78.

11. R. DINIZ and A. DOS SANTOS, "A Noise Analysis Approach for Measuring the Decay Constants and the Relative Abundance of Delayed Neutrons in a Zero Power Critical Facility," *J. Nucl. Sci. Technol.*, Suppl. 2, 669 (Aug. 2002).

12. R. DINIZ and A. DOS SANTOS, "Experimental Determination of the Decay Constants and Abundances of Delayed Neutrons by Means of Reactor Noise Analysis," *Nucl. Sci. Eng.*, **152**, 125 (2006); http://dx.doi.org/10.13182/NSE04-69.

13. R. Y. R. KURAMOTO et al., "Absolute Measurement of β_{eff} Based on Rossi-α Experiments and the Two-Region Model in the IPEN/MB-01 Research Reactor," *Nucl. Sci. Eng.*, **158**, *3*, 272 (2008); http://dx.doi.org/10.13182/NSE06-120.

14. R. Y. R. KURAMOTO et al., "Absolute Measurement of β_{eff} Based on Feynman-α Experiments and the Two-Region Model in the IPEN/MB-01 Research Reactor," *Ann. Nucl. Energy*, **34**, *6*, 433 (2006); http://dx.doi.org/10.1016/j.anucene.2007.02.012.

15. A. SANTAMARINA et al., "Calculation of LWR β_{eff} Kinetic Parameters: Validation on the MISTRAL Experimental Program," *Ann. Nucl. Energy*, **48**, 51 (2012); http://dx.doi.org/10.1016/j.anucene.2012.05.001.

16. P. HUMBERT, "Third Order Time Correlation Method Applied to Silene Absolute Criticality Measurements," *Proc. Advances in Reactor Physics to Power the Nuclear Renaissance (PHYSOR 2010)*, Pittsburgh, Pennsylvania, May 9–14, 2010, American Nuclear Society (2010).

17. A. DOS SANTOS et al., "A New Experimental Approach for Subcritical Reactivity Determination of Multiplying Systems," *Ann. Nucl. Energy*, **59**, 243 (2013); http://dx.doi.org/10.1016/j.anucene.2013.04.015.

18. J. HARDY, "ENDF/B Data Testing Results for Thermal Reactor Benchmark," *Proc. Thermal Reactors Benchmark Calculations: Techniques, Results, and Applications*, EPRI-NP-2885, Bettis Atomic Power Laboratory (Feb. 1983).

19. F. RAHNEMA and S. McKINLEY, "On the Validation of ENDF/B-VI Nuclear Data for Light Water Reactor Criticality Analysis," *Ann. Nucl. Energy*, **24**, *14*, 1151 (1997); http://dx.doi.org/10.1016/S0306-4549(97)00036-4.

20. J. HARDY and A. C. KAHLER, "Analysis of Benchmark Critical Experiments with ENDF/B-VI Data Sets," *Proc. Int. Topl. Mtg. Advances in Mathematic Computations and Reactor Physics*, Pittsburgh, Pennsylvania, April 28–May 2, 1991, p. 19.1 1-1, American Nuclear Society (1991).

21. J. L. IVERSON and R. D. MOSTELLER, "Results of MCNP Calculations for Criticality Safety Benchmarks with ENDF/B-V and ENDF/B-VI Libraries," *Trans. Am. Nucl. Soc.*, **72**, 199 (1995).

22. N. D. KEEN, S. C. FRANKLE, and R. E. MacFARLANE, "Criticality Benchmark Results for the ENDF60 Library with MCNP," *Trans. Am. Nucl. Soc.*, **73**, 216 (1995).

23. *International Handbook of Evaluated Criticality Safety Benchmark Experiments (ICSBEP)*, NEA/NSC/DOC (95)03/I, J. B. BRIGGS, Ed., Nuclear Energy Agency (Sep. 2012).

24. *International Handbook of Evaluated Reactor Physics Benchmark Experiments (IRPhEP)*, NEA/NSC/DOC(2006)1, J. B. BRIGGS, Ed., Nuclear Energy Agency (Mar. 2012).

25. S. C. VAN DER MARCK, "Benchmarking ENDF/B-VII.1, JENDL-4.0 and JEFF-3.1.1 with MCNP6," *Nucl. Data Sheets*, **113**, 2935 (2012); http://dx.doi.org/10.1016/j.nds.2012.11.003.

26. S. C. VAN DER MARCK and A. HOGENBIRK, "Criticality Results for Many Benchmark Cases—The Releases JEFF-3.0, ENDF/B-VI.8, JENDL-3.3, ENDF-B/VII-prelim," JEFDOC 974, Nuclear Energy Agency (2003).

27. A. C. KAHLER et al., "ENDF/B-VII.1 Neutron Cross Section Data Testing with Critical Assembly Benchmarks and Reactor Experiments," *Nucl. Data Sheets*, **112**, 2997 (2011); http://dx.doi.org/10.1016/j.nds.2011.11.003.

28. S. C. VAN DER MARCK "β_{eff} Calculations Using JEFF-3.1 Nuclear Data," NRG Report 21616/05.69454/P (also published as JEF/DOC-1105), Nuclear Research and Consultancy Group (2005); see also S. C. VAN DER MARCK, "Shielding Benchmark Calculations with MCNP-4C3 Using JEFF-3.1 Nuclear Data," NRG Report 21616/05.69455/P (also published as JEF/DOC-1106), Nuclear Research and Consultancy Group (2005); see also S. C. VAN DER MARCK, "Criticality Safety Benchmark Calculations with MCNP-4C3 Using JEFF-3.1 Nuclear Data," NRG Report 21616/05.69456/P (also published as JEF/DOC-1107), Nuclear Research and Consultancy Group (2005).

29. A. D'ANGELO, "Overview of the Delayed Neutron Data Activities and Results Monitored by the NEA/WPEC Subgroup 6," *Prog. Nucl. Energy*, **41**, *1–4*, 5 (2002); http://dx.doi.org/10.1016/S0149-1970(02)00004-5.

30. T. SAKURAI et al., "Experimental Cores for Benchmark Experiments of Effective Delayed Neutron Fraction β_{eff} at FCA," *Prog. Nucl. Energy*, **35**, *2*, 131 (1999); http://dx.doi.org/10.1016/S0149-1970(99)00007-4.

31. G. RUDSTAN et al., "Delayed Neutron Data for the Major Actinides," NEA/WPEC-6 Report, Working Party on International Evaluation Co-operation of the NEA Nuclear Science Committee (2002).

32. A. D'ANGELO and J. L. ROWLANDS, "Conclusions Concerning the Delayed Neutron Data for the Major Actinides," *Prog. Nucl. Energy*, **41**, *1–4*, 391 (2002); http://dx.doi.org/10.1016/S0149-1970(02)00020-3.

33. S. VAN DER MARCK et al., "Benchmark Results for Delayed Neutron Data," *Proc. Int. Conf. Nuclear Data for Science and Technology*, Santa Fe, New Mexico, September 26–October 1, 2004.

34. S. VAN DER MARCK, "β_{eff} Calculations Using ENDF/B-VII beta2 Nuclear Data," NRG 21616/05.70024/P, Nuclear Research and Consultancy Group (June 13, 2006).

35. V. A. DUKIN, "Measurement of the Effective Delayed-Neutron Dose by the α-Rossi Method in Water-Containing Media," *At. Energ.*, **100**, *5*, 370 (2006); http://dx.doi.org/10.1007/s10512-006-0096-2.

36. G. D. SPRIGGS et al., "Two-Region Kinetic Model for Reflected Reactors," *Ann. Nucl. Energy*, **24**, *3*, 205 (1997); http://dx.doi.org/10.1016/0306-4549(96)00062-X.

37. M. BRUGGEMAN et al., "Neutron Coincidence Counting Based on Time Interval Analysis with One- and Two-Dimensional Rossi-Alpha Distributions: An Application for Passive Neutron Waste Assay," *Nucl. Instrum. Methods Phys. Res., Sect. A*, **382**, 511 (1996); http://dx.doi.org/10.1016/S0168-9002(96)00795-4.

38. R. E. UHRIG, *Random Noise Techniques in Nuclear Reactor System*, The Ronald Press Company (1970).

39. T. GOORLEY et al., "Initial MCNP6 Release Overview," *Nucl. Technol.*, **180**, *3*, 298 (2012); http://dx.doi.org/10.13182/NT11-135.

40. A. DOS SANTOS et al., "IPEN (MB01)-LWR-CRIT-BUCK-SPEC-REAC-COEF-KIN-RRATE-POWDIS, Reactor Physics Experiments in the IPEN/MB-01 Research Reactor Facility," *International Handbook of Evaluated Reactor Physics Benchmark Experiments*, Nuclear Energy Agency (Mar. 2012).

41. C. E. COHN, "A Simplified Theory of Pile Noise," *Nucl. Sci. Eng.*, **7**, 472 (1960); http://dx.doi.org/10.13182/NSE60-4.

42. *Noise Analysis in Nuclear Systems; Proceedings of a Symposium Held at the University of Florida*, November 4–6, 1963, R. E. UHRIG, Ed., U.S. Atomic Energy Commission.

43. E. SUZUKI, "A Method for Measuring Absolute Reactor Power Through Neutron Fluctuation," *J. Nucl. Sci. Technol.*, **3**, *3*, 98 (1966); http://dx.doi.org/10.1080/18811248.1966.9732284.

44. J. R. THOMAS, JR., J. D. HERR, and D. S. WOOD, "Noise Analysis Method for Monitoring the Moderator Temperature Coefficient of Pressurized Water Reactors: I. Theory," *Nucl. Sci. Eng.*, **108**, 331 (1991), http://dx.doi.org/10.13182/NSE90-42; see also J. D. HERR and J. R. THOMAS, JR., "Noise Analysis Method for Monitoring the Moderator Temperature Coefficient of Pressurized Water Reactors: II. Experimental," *Nucl. Sci. Eng.*, **108**, 341 (1991), http://dx.doi.org/10.13182/NSE90-43.

45. E. J. M. WALLERBOS and J. E. HOOGENBOOM, "The Measurement and Calculations of the Kinetic Parameter β_{eff}/Λ of a Small High-Temperature Like, Critical System," *J. Nucl. Sci. Technol.*, **35**, *1*, 26 (1998); http://dx.doi.org/10.1080/18811248.1998.9733816.

46. M. M. R. WILLIAMS, *Random Processes in Nuclear Reactors*, Pergamon Press (1974).

47. A. DOS SANTOS et al., "LEU-COMP-THERM-077: Critical Loading Configurations of the IPEN/MB-01 Reactor," *International Handbook of Evaluated Criticality Safety Benchmark Experiments*, NEA/NSC/DOC (95)03/I, J. B. BRIGGS, Ed., Nuclear Energy Agency (Sep. 2013).

48. A. DOS SANTOS et al., "LEU-COMP-THERM-082: Critical Loading Configurations of the IPEN/MB-01 Reactor with Low Enriched Fuel and Burnable Poison Rods," *International Handbook of Evaluated Criticality Safety Benchmark Experiments*, NEA/NSC/DOC (95)03/I, J. B. BRIGGS, Ed., Nuclear Energy Agency (Sep. 2013).

49. A. DOS SANTOS et al., "A Proposal of a Benchmark for β_{eff}, β_{eff}/Λ and Λ of Thermal Reactors Fueled with Slightly Enriched Uranium," *Ann. Nucl. Energy*, **33**, 848 (2006); http://dx.doi.org/10.1016/j.anucene.2006.03.006.

50. "ENDF/B-VI Summary Documentation," BNL-NCS-17451 (ENDF-201) (Release-8), 4th ed. (ENDF/B-VI), P. F. ROSE, Ed., National Nuclear Data Center, Brookhaven National Laboratory (2000).

51. ENDF/B-VI.8 (LANL Review): http://www.oecd-nea.org/dbforms/data/eva/evatapes/ (current as of Jan. 10, 2014).

52. T. NAKAGAWA et al., "Japanese Evaluated Nuclear Data Library Version 3 Revision-2: JENDL-3.2," *J. Nucl. Sci. Technol.*, **32**, 1259 (1995); http://dx.doi.org/10.1080/18811248.1995.9731849.

53. W. H. PRESS, *Numerical Recipes*, Cambridge University Press (1992).

54. A. DOS SANTOS et al., "The Application of the Multiple Transient Technique for the Experimental Determination of the Relative Abundances and Decay Constants of Delayed Neutrons of the IPEN/MB-01 Reactor," *Ann. Nucl. Energy*, **33**, 917 (2006); http://dx.doi.org/10.1016/j.anucene.2006.04.010.

55. J. S. BENDAT and A. G. PIERSOL, *Random Data—Analysis and Measurement Procedures*, 2nd ed., John Wiley, New York (1986).

56. C. JAMMES et al., "First MUSE-4 Experimental Results Based on Time Series Analysis," *Proc. PHYSOR 2002*, Seoul, Korea, October 7–10, 2002.

57. T. MISAWA and H. UNESAKI, "Measurement of Subcriticality by Higher Mode Source Multiplication Method," *Proc. 7th Int. Conf. Nuclear Criticality Safety (ICNC2003)*, Tokai-mura, Japan, October 2003.

58. Y.-Q. SHI, Q.-F. ZHU, and H. TAO, "Review and Research of the Neutron Source Multiplication Method in Nuclear Critical Safety," *Nucl. Technol.*, **149**, *1*, 122 (2005); http://dx.doi.org/10.13182/NT05-2.

59. P. R. BEVINGTON, *Data Reduction and Error Analysis for Physical Sciences*, McGraw-Hill (1969).

60. J. BARHEN, W. RHOTENSTEIN, and E. TAVIV, "The Hammer Code System," NP-565, Technion-Israel Institute of Technology (Oct. 1978).

61. T. B. FOWLER, D. R. VONDY, and G. W. CUNNINGHAM, "Nuclear Reactor Core Analysis Code: CITATION," ORNL-2496, Version 2, Oak Ridge National Laboratory (1971).

62. G. I. BELL and S. GLASSTONE, *Nuclear Reactor Theory*, Van Nostrand Reinhold, New York (1979).

63. M. B. CHADWICK et al., "ENDF/B-VII.0: Next Generation Evaluated Nuclear Data Library for Nuclear Science and Technology," *Nucl. Data Sheets*, **107**, 2931 (2006); http://dx.doi.org/10.1016/j.nds.2006.11.001.

64. M. B. CHADWICK et al., "ENDF/B-VII.1 Nuclear Data for Science and Technology: Cross Sections, Covariances, Fission Product Yields and Decay Data," *Nucl. Data Sheets*, **112**, 2887 (2011); http://dx.doi.org/10.1016/j.nds.2011.11.002.

65. A. SANTAMARINA, D. BERNARD, and Y. RUGAMA, "The JEFF3.1.1 Nuclear Data Library," JEFF Report 22, Organisation for Economic Co-operation and Development/Nuclear Energy Agency (2009).

66. K. SHIBATA et al. "JENDL-4.0: A New Library for Nuclear Science and Engineering," *J. Nucl. Sci. Technol.*, **48**, 1 (2011); http://dx.doi.org/10.1080/18811248.2011.9711675.

67. *Handbook of Chemistry and Physics*, 70th ed., R. C. WEAST, Ed., CRC Press (1989).